PNAS RESEARCH ARTICLE | DEVELOPMENTAL BIOLOGY

Cohesin controls X chromosome structure remodeling and X-reactivation during mouse iPSC-reprogramming

Serena F. Generoso[a], Maria Victoria Neguembor[a,1], Elliot A. Hershberg[b], Ruslan I. Sadreyev[c,d], Kazuki Kurimoto[e,f,g], Yukihiro Yabuta[e,f,g], Raffaele Ricci[a], Pauline Audergon[a], Moritz Bauer[h], Mitinori Saitou[e,f,g], Konrad Hochedlinger[c,i], Brian J. Beliveau[b], Maria Pia Cosma[a,j,k], Jeannie T. Lee[c,l,1], and Bernhard Payer[a,j,1]

Contributed by Jeannie T. Lee; received August 11, 2022; accepted December 14, 2022; reviewed by Irene Cantone, Azusa Inoue, and Ana Losada

Reactivation of the inactive X chromosome is a hallmark epigenetic event during reprogramming of mouse female somatic cells to induced pluripotent stem cells (iPSCs). This involves global structural remodeling from a condensed, heterochromatic into an open, euchromatic state, thereby changing a transcriptionally inactive into an active chromosome. Despite recent advances, very little is currently known about the molecular players mediating this process and how this relates to iPSC-reprogramming in general. To gain more insight, here we perform a RNAi-based knockdown screen during iPSC-reprogramming of mouse fibroblasts. We discover factors important for X chromosome reactivation (XCR) and iPSC-reprogramming. Among those, we identify the cohesin complex member SMC1a as a key molecule with a specific function in XCR, as its knockdown greatly affects XCR without interfering with iPSC-reprogramming. Using super-resolution microscopy, we find SMC1a to be preferentially enriched on the active compared with the inactive X chromosome and that SMC1a is critical for the decompacted state of the active X. Specifically, depletion of SMC1a leads to contraction of the active X both in differentiated and in pluripotent cells, where it normally is in its most open state. In summary, we reveal cohesin as a key factor for remodeling of the X chromosome from an inactive to an active structure and that this is a critical step for XCR during iPSC-reprogramming.

cellular reprogramming | X chromosome | X-reactivation | cohesin | X-inactivation

Significance

The X chromosome in female mammals exists in two states: as compacted, transcriptionally inactive and as decompacted, active chromosome. During reprogramming of differentiated cells into induced pluripotent stem cells, the inactive X gets switched on by X chromosome reactivation (XCR). Until now, it was not understood which molecules control XCR and how this is linked with stem cell reprogramming. Here we identify the cohesin protein SMC1a as a key regulator of this process. Reducing SMC1a levels by RNA-interference did not disrupt stem cell reprogramming overall, but greatly impaired restructuring of the X chromosome and turning on its genes during XCR. Thereby we revealed a mechanism how an entire chromosome can change its 3D-structure and be switched from "OFF" to "ON."

Mammals avoid a sex chromosome dosage imbalance between males and females by transcriptionally inactivating one of the two X chromosomes in females (1–3). However, X-inactivation is reversed twice during mouse development by a process termed X chromosome reactivation (XCR) (4–6); first in the late epiblast of preimplantation blastocysts (7–10) and later in the germ cell lineage (11–14). In the epiblast, reactivation of the imprinted inactive X is restricted to cells expressing the pluripotency factor NANOG, thus linking XCR to the naive pluripotent cell fate (7, 9, 15). Also in vitro, XCR is coupled to the acquisition of pluripotency, either when somatic cells are fused with pluripotent stem cells (16, 17) or during induced pluripotent stem cell (iPSC)-reprogramming (9, 18–21). An essential step linking XCR to pluripotency is the downregulation of the X-inactivation master regulator and long noncoding RNA Xist (19), which is mediated by pluripotency factors such as OCT4, NANOG, or PRDM14 (9, 22–24) when they become endogenously expressed during reprogramming (19, 21). Nevertheless, to what extent XCR is in turn important for the acquisition of pluripotency during iPSC-reprogramming, remains unclear.

Apart from *Xist* downregulation, XCR is a multistep process, which involves global remodeling of the X chromosome 3D-structure, and chromatin state leading eventually to transcriptional reactivation of X-linked genes. The inactive X chromosome (Xi) thereby loses repressive chromatin marks such as H3K27me3 and DNA methylation at X-linked gene promoters and gains active marks such as histone acetylation (18–20). Furthermore, during this transition from a heterochromatic Xi to an euchromatic active X (Xa), chromatin opening occurs, initially starting from already open escapee regions and then further progressing along the entire chromosome (21, 25). Judging from the speed at which these chromatin changes take place—in vivo in the epiblast even within one day without significant cell proliferation—suggests active mechanisms to be at play. For example, efficient removal of the H3K27me3 mark during XCR from the Xi requires the histone demethylase KDM6A/UTX (10), and gene reactivation is promoted by inhibition of DNA-methyltransferases and histone deacetylases (19, 20, 26).

The Xi is distinguished from the Xa and autosomes by substantial 3D-structural differences, and therefore XCR requires dramatic rewiring of X chromosome topology. A characteristic Xi feature is its packaging into two so-called megadomains separated by

Reviewers: I.C., Universita degli Studi di Napoli Federico II Dipartimento di Medicina Molecolare e Biotecnologie Mediche; A.I., RIKEN; and A.L., Centro Nacional de Investigaciones Oncologicas.

Competing interest statement: J.T.L. is a cofounder of Fulcrum Therapeutics and is also a scientific advisor to Skyhawk Therapeutics. The authors declare that the research was conducted in the absence of any commercial or financial relationships that could be construed as a potential conflict of interest.

[1]To whom correspondence may be addressed. Email: victoire.neguembor@crg.eu, lee@molbio.mgh.harvard.edu, or bernhard.payer@crg.eu.

This article contains supporting information online at https://www.pnas.org/lookup/suppl/doi:10.1073/pnas.2213810120/-/DCSupplemental.

Published January 20, 2023.

the macrosatellite repeat boundary element *Dxz4* (27–30). Furthermore, topological domains and loops, which are bound by the structural factor CTCF and are generated by chromatin loop extrusion by cohesin proteins, are strongly attenuated on the Xi (29–31). Xist RNA binds and repels cohesin and CTCF from the Xi (29, 32), and downregulation of Xist during XCR leads to the reappearance of topological domains on the reactivated Xa (21). Furthermore, chromosome compartments, which structurally separate domains of different chromatin states (27, 31, 33, 34), become remodeled during reprogramming to pluripotency and specifically influence the reactivation kinetics of X-linked genes (21).

Although much has been recently learned by kinetic studies of XCR during iPSC-reprogramming (19–21, 25), little is known about the molecules, which functionally drive the process of transforming the X chromosome from an inactive into an active state. Furthermore, a clear understanding has been lacking, if factors regulating XCR would also affect iPSC-reprogramming in general, or if the two processes would remain functionally separated. To gain further insights into these questions, we here performed a functional knockdown screen during iPSC-reprogramming and thereby identified factors important for XCR and pluripotency acquisition. Among them, we found that the cohesin complex member SMC1a is a factor that plays a critical role in XCR. The importance of cohesins has been widely established for genome structure (35) and in particular in the context of X chromosome structure during X-inactivation, where cohesin gets specifically evicted from the inactive X chromosome by Xist RNA (29, 32). However, to which degree the deposition of cohesin molecules on the X chromosome is functionally important for the reestablishment of an active 3D-structure during XCR and if this would impact the reactivation of X-linked genes was previously unknown. Furthermore, while some prior studies on cohesin and pluripotency suggested a direct role in pluripotency gene regulation and reprogramming (36–38), others proposed these effects to be rather indirect through cell cycle-related functions of cohesin such as controlling cell proliferation and DNA damage (39, 40). Up till now, it has never been addressed, if cohesin affected XCR during reprogramming and if this would impact pluripotency acquisition. Here we found that while knockdown of Smc1a and other cohesin complex members led to diminished reactivation of an X-linked GFP reporter (41) and the endogenous X chromosomal gene *Hprt*, cohesin depletion did not affect the formation of iPSC colonies. This suggests that cohesin has a predominant role in XCR and that iPSC formation is not dependent on XCR in female cells, thus uncoupling the two events mechanistically. Furthermore, using super-resolution (SR) microscopy we see preferential binding of SMC1a to the Xa in comparison to the Xi at the single-cell level. Finally, we show that SMC1a is critical to guarantee the decompacted state of the Xa in both differentiated cells and pluripotent stem cells. Thus our study reveals how remodeling of X chromosome structure by SMC1a is a critical step for switching the X chromosome from a silent to an active state during reprogramming.

Results

Functional shRNA-Knockdown Screen during iPSC-Reprogramming Identifies SMC1a as a Regulator of XCR. Transcriptional reactivation of the paternal X chromosome (Xp) in vivo occurs in specific cells of the mouse blastocyst between E(embryonic day)3.5 and E4.5 during pre- to periimplantation development. While the trophectoderm (TE) and the primitive endoderm (PE) maintain Xist RNA expression and thereby imprinted silencing of genes on the Xp, the epiblast cells within the inner cell mass (ICM) gradually down-regulate Xist and undergo XCR (7, 8, 10). To identify genes with potential roles in the XCR process, we performed single-cell expression profiling of ICM cells of blastocysts prior (E3.5, EPI Xist+), during (E4.25, EPI Xist+/Xist-) and after (E4.5, EPI Xist-) XCR. Combining our own data with a published dataset (42), we ranked genes by Pearson correlation with *Xist* expression in epiblast cells over time, based on the assumption that genes actively involved in XCR would be progressively up-regulated in epiblast between E3.5 and E4.5 and thus anticorrelated with Xist (Dataset S1). We then went on to choose genes based on the type of factor encoded and their potential involvement in XCR and added selected candidate genes from the literature, which were expressed in epiblast, resulting in a list of 56 candidate genes, which we grouped into four main categories: transcription regulators, chromatin factors, signaling, and others (*SI Appendix,* Table S1). This candidate list provided our basis for an shRNA screen to identify regulators of XCR during the reprogramming to iPSCs (Fig. 1 *A* and *B*), which has been previously used as in vitro system for studying mechanisms of XCR (9, 18–21, 25). We first performed a primary shRNA screen in female mouse embryonic fibroblasts (MEFs) undergoing reprogramming to iPSCs. We therefore derived MEFs from reprogrammable mice harboring a doxycycline (dox)-inducible polycistronic *OKSM* (*Oct4, Klf4, Sox2, c-myc*) cassette (43) and carrying a *GFP* transgene on one X chromosome as a reporter for X-activity (41) and a mutation of the hypoxanthine-guanine phosphoribosyltransferase (*Hprt*) gene on the other X (44). This enabled us to isolate by FACS XGFP–MEFs, which harbored the *XGFP* transgene on the inactive X chromosome (Xi) as starting material for our reprogramming experiments. As it has been previously shown that the *XGFP* transgene can be also silenced independently of X-inactivation when located on the active Xa (45), we used a selection approach based on the X-linked *Hprt* gene (see *Methods*) to remove those cells in the 6-thio-guanine (6TG) medium and ensure a pure starting population of $Xi^{GFP}Xa^{Hprt-}$ cells. This ensured that the XGFP-readout reflected the activity of the transgene-harboring X chromosome and not nonspecific transgene silencing.

The 6TG-selected, XGFP–MEFs were then transduced with lentiviral hairpins targeting the 56 candidate genes with three different shRNAs for each gene or control shRNAs on a well-by-well basis and treated with Dox to induce reprogramming (Fig. 1*B*). The first colonies emerged after 4 to 5 d of OKSM expression leading to fully reprogrammed iPSCs around day 14. The first evidence of *XGFP* reactivation was visible around day 8, when few cells within the colonies started to become green and reached the highest levels at the end point of the reprogramming time course when colonies were almost completely green (Fig. 1*C*). We then analyzed the impact of candidate gene knockdown on iPSC-reprogramming efficiency by counting the number of colonies and normalizing it to the nontargeting LacZ shRNA as negative control (Fig. 1*D*). Knockdown of the reprogramming factor Oct4 (46) resulted in low reprogramming efficiency as expected. On the other hand, knockdown of Tcf3, a known repressor of reprogramming (47, 48), led to increased reprogramming efficiency. Since most of the selected candidates are up-regulated in the pluripotent epiblast lineage, which is the precursor of all embryonic cell types and from which pluripotent embryonic stem cells (ESCs) are derived, we expected some of them to have a role in pluripotency and somatic cell reprogramming. Indeed, we observed that the knockdown of the majority of the candidates decreased the efficiency of reprogramming compared to LacZ shRNA (Fig. 1*D* and Dataset S2). As our main goal was to identify regulators of XCR, we then focused on factors whose knockdown caused reduced *XGFP* reactivation (Fig. 1*E*). As expected, control

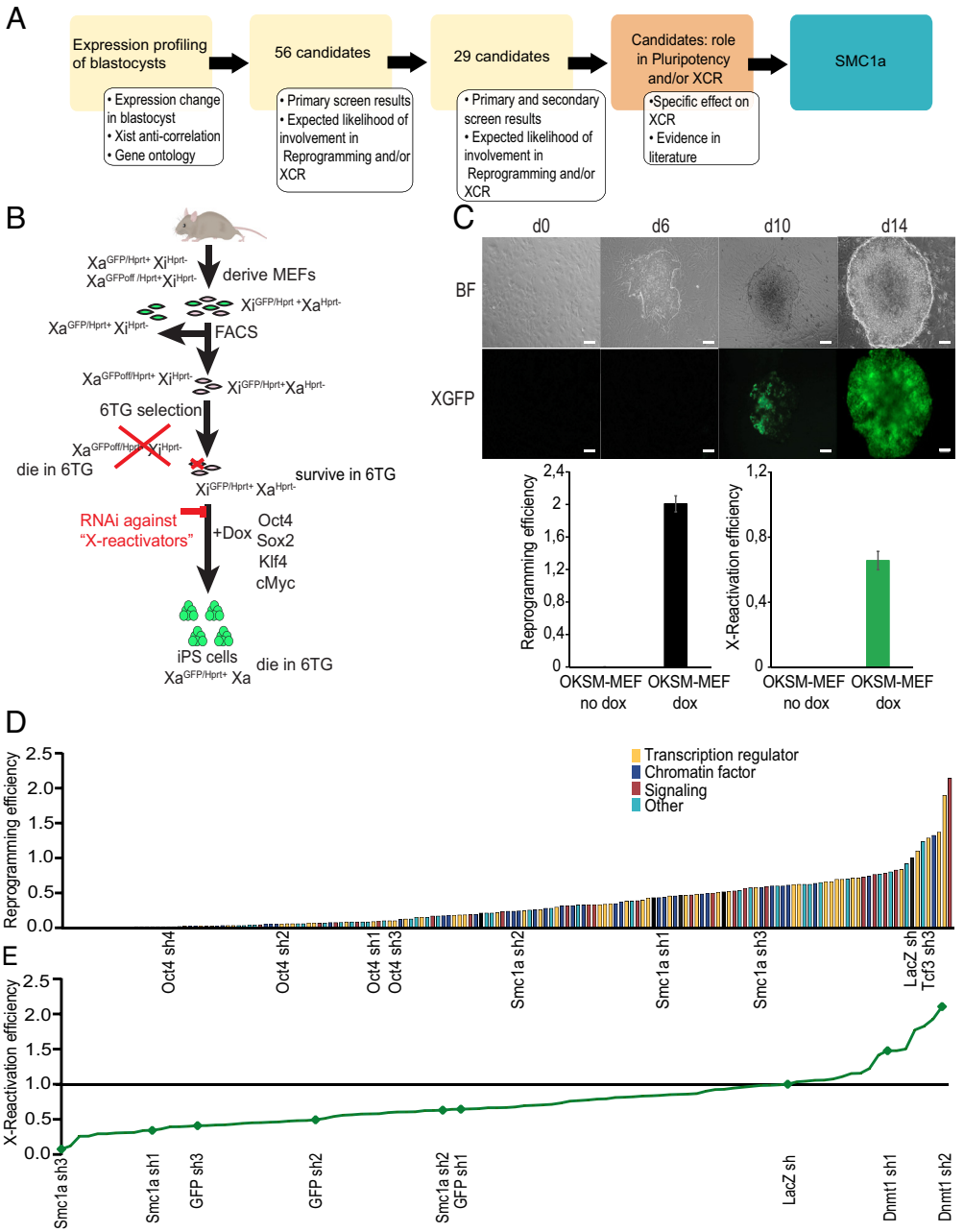

Fig. 1. Functional shRNA-knockdown screen reveals that SMC1a knockdown affects X-reactivation. (*A*) Steps of the screening process. (*B*) Experimental design of the screen work-flow. (*C*) Characterization of the *XGFP*/*OKSM*-MEF iPSC-reprogramming system. Representative images of reprogramming time points (d0-d6-d10-d14) showing the colony formation in brightfield (BF) and the XGFP reactivation in green (Scale bars = 50 μm.) Reprogramming efficiency (*Left* quantification graph) was scored as the percent of primary colonies formed per input MEFs after 14 d of dox induction. X-Reactivation efficiency (*Right* graph) was scored as ratio between XGFP+ colonies and total colony number. Each graph depicts data from one experiment performed in triplicate (error bars = SEM). (*D*) Reprogramming efficiency upon shRNA knockdowns scored as the total colony number divided by the seeded cell number and normalized to LacZ shRNA as negative control (set as 1). Each bar is depicted in different colors according to Gene Ontology analysis. Black bars show shRNAs controls. (*E*) XCR efficiency scored as ratio between XGFP positive colony number and the total colony number and normalized to LacZ shRNA as a control (set as 1).

hairpins against *GFP* reduced the frequency of GFP+ colonies. On the contrary, knockdown of the DNA methyltransferase Dnmt1 resulted in a clear increase in *XGFP* reactivation, in agreement with the role of Dnmt1 in the maintenance of X-inactivation (26, 49). Among our candidates which showed a consistent decrease in *XGFP* reactivation upon knockdown was the cohesin complex member Smc1a. In fact, Smc1a knockdown showed a comparable impact on *XGFP*-reactivation as knockdown of GFP itself (Fig. 1*E* and Dataset S2), suggesting a role for SMC1a in the reactivation process. In order to narrow down the number of candidates and validate our results, we performed a secondary validation screen using the same system and replacing some of the hairpins, which were either toxic or ineffective during the primary screen. We focused on the factors that were selected according to their effect on XCR preferentially and on both XCR and pluripotency across replicates with at least two out of three hairpins (*SI Appendix*, Fig. S1 *A* and *B*) and also checked the knockdown efficiency of the selected hairpins (*SI Appendix*, Fig. S1*C*). Confirming the results from our primary screen, knockdown of many of the candidates resulted in reduced pluripotent colony formation in accordance with their upregulation in the epiblast (*SI Appendix*, Fig. S1*A* and Dataset S2). Knockdown of Smc1a, however, did not greatly affect the capability of the cells to reprogram but rather impaired their capacity to undergo XCR based

on *XGFP* reactivation (*SI Appendix*, Fig. S1*B* and Dataset S2). In summary, through our screen we identified genes with potential roles during reprogramming and XCR and found the cohesin complex member SMC1a to be particularly important for the XCR process.

SMC1a Promotes X-Linked Gene Reactivation during iPSC-Reprogramming. Our iPSC-screening system is based on reactivation of *XGFP*, a transgene inserted into the X chromosome by random integration (41), as a simple readout for XCR. To confirm that our XCR screening results based on the *XGFP* readout reflect the reactivation of endogenous X-linked genes, we took advantage of the fact that our reprogrammable MEFs also have a mutation of the endogenous *Hprt* allele on the opposite X chromosome to the *XGFP*-harboring one (44, 45). As we selected initially for $Xa^{Hprt-}/Xi^{GFP/Hprt+}$ MEFs by culturing them in the 6TG medium, which kills cells with an active *Hprt* wild-type allele (Fig. 1*B*), after reprogramming, iPSCs, which have undergone XCR would become $Xa^{Hprt-}/Xa^{GFP/Hprt+}$ and thereby sensitive to 6TG (Fig. 2*A*). In contrast, iPSCs which failed to undergo XCR and reactivate the *Hprt*+ allele ($Xa^{Hprt-}/Xi^{GFP/Hprt+}$) would survive. This allowed us to test the impact of knockdown of our candidate genes on XCR during reprogramming using both *XGFP*-reactivation, as well as reactivation of the endogenous X-linked gene *Hprt* (lethality in 6TG) as a readout. Following iPSC-reprogramming until day 10, we reseeded the colonies on *Hprt* (–) 6TG-resistant feeders, applied 6TG selection to iPSCs for 6 d, and quantified by flow cytometry surviving iPSCs based on the pluripotency markers EpCAM1 and SSEA1 (50) (Fig. 2 *A* and *B*). As expected, almost only *XGFP*-negative cells were able to survive, indicating that *XGFP*-reactivation was a good proxy for reactivation of endogenous X-linked genes like *Hprt* (*SI Appendix*, Fig. S2*A* and Dataset S3). Furthermore, control knockdowns of lacZ or repressors of XCR such as Dnmt1 and Tcf3 resulted in no iPSCs surviving, indicating that they have all undergone XCR and were eliminated during 6TG selection (Fig. 2*B*). On the contrary, knockdown of the candidates, which emerged from the primary and secondary screens as being important for XCR such as Smc1a, resulted frequently in iPSCs surviving 6TG selection (Fig. 2*B*), which also remained XGFP-negative indicating a lack of XCR (*SI Appendix*, Fig. S2*A* and Dataset S2). This thereby validated several of our candidates including SMC1a as factors with a functional role in XCR.

Downregulation of Xist RNA, the master-regulator of X-inactivation, is an essential step during XCR (9, 10, 18–21) and several of our candidates showed anticorrelation with *Xist* downregulation in the mouse epiblast (Dataset S1). Therefore, we wanted to investigate if our candidate factors' role for promoting XCR was directly repressing *Xist*. For that reason, we knocked down the 29 XCR candidate factors, which emerged from the primary screen in ESCs, where *Xist* is not expressed, and quantified its derepression by qRT-PCR (Fig. 2*C*). After knocking down factors such as Nanog and Oct4 (Fig. 2*C*), whose role in *Xist* repression has been previously described (22, 51), we observed a clear upregulation of *Xist* in ESCs. However, we did not see a clear derepression of *Xist* when knocking down our candidate genes. Furthermore, we looked at expression of Tsix, which is a negative regulator of *Xist* and has been implicated in XCR in mouse blastocysts (9) (*SI Appendix*, Fig. S2*B*). While we observed reduced Tsix expression after knocking down Zfp42/Rex1, a known activator of *Tsix* (52), we did not see a consistent downregulation of *Tsix* after knock-down of our other candidates. We also examined expression of *Rnf12/Rlim*, a positive regulator of *Xist* (53), and only saw some increase in Rnf12 expression when we knocked down Oct4, a known repressor of *Rnf12* (24) (*SI Appendix*, Fig. S2*C*). In conclusion, although many of our candidate factors display an anticorrelation with *Xist* expression during XCR in blastocysts (Dataset S1), they do not seem to control XCR by derepressing *Xist* or by modulating expression of the *Xist* regulators *Tsix* and *Rnf12*. This suggests our XCR candidates, including Smc1a, rather promote XCR by other, Xist-independent mechanisms.

Cohesin Knockdown Impairs XCR but Not iPSC-Reprogramming Efficiency. Throughout the different screening runs, it emerged consistently that knockdown of the cohesin subunit SMC1a strongly reduced XCR efficiency while having little effect on the formation of iPSC colonies (Figs. 1 *D* and E and 2 *B* and *SI Appendix*, Figs. S1 *A* and *B* and S2*A*). As the cohesin complex plays many key roles in cell cycle, DNA repair, and genome organization (54), we further wanted to discriminate between a more general reprogramming phenotype and a specific effect on XCR and therefore focused our attention on the core components of the cohesin complex SMC1a, SMC3, and RAD21 (35). We first performed knockdown of cohesin complex members during iPSC reprogramming from male MEFs (Fig. 3 *A*–*C* and *SI Appendix*, Fig. S3*A*), which allowed us to assess the effect on colony formation only, as XCR does not occur in male cells. While Oct4 depletion strongly impaired reprogramming in male cells, Smc1a, Rad21, and Smc3 knockdown did not consistently affect the number of colonies formed compared with LacZ control (Fig. 3*A*). Moreover, when we assessed the percentage of iPSCs based on the surface markers EpCAM1 and SSEA1 at day 11, we only observed relatively minor effects, when compared with Oct4 knockdown, which greatly diminished reprogramming efficiency (Fig. 3 *B* and *C*). This is in line with previous studies, which reported that cohesins were not required for pluripotency gene reactivation during reprogramming by somatic cell–pluripotent stem cell fusion (39, 40).

We then went on to examine the effect of cohesin depletion on iPSC reprogramming and XCR of female MEFs (Fig. 3 *D*–*I* and *SI Appendix*, Fig. S3*B*). By imaging, we could see that in female cells colony formation was not impaired after cohesin complex members' knockdown, whereas *XGFP* reactivation was greatly reduced (Fig. 3*D*). We observed a slight but not significant decrease in terms of colony number upon cohesin knockdown, similar to what we observed in the previous screening rounds for Smc1a (Figs. 1*D* and 3*E* and *SI Appendix*, Fig. S1*A*). However, when we looked at XCR based on *XGFP* reactivation, we observed a highly significant reduction in XGFP-positive colonies for Smc1a shRNA compared with LacZ control (Fig. 3*F*). A similar reduction in *XGFP* reactivation was observed upon Smc3 and Rad21 depletion suggesting a general role for the cohesin complex during XCR. We then further quantified the effects by FACS analysis and looked at iPSC reprogramming efficiency based on the pluripotency markers EpCAM1 and SSEA1 and XCR based on the percentage of XGFP+ iPSCs (Fig. 3*G*). As for colony numbers, we did not observe a major impairment of pluripotency acquisition based on SSEA1/EpCAM1 FACS upon cohesins' knockdown (Fig. 3*H*). However, we could detect a significant decrease in the percentage of XGFP-positive cells within the EpCAM1+/SSEA1+ double-positive population (Fig. 3*I*). While in the LacZ shRNA control, the percentage of XGFP+ pluripotent cells was around 37%, in Smc1a knockdown cells the percentage dropped to on average of 18%. Rad21 and Smc3 knockdown showed similar effects on *XGFP* reactivation (Fig. 3 *G*–*I*). It is important to stress that we observed these results after incomplete depletion of cohesins by shRNA knockdown (*SI Appendix*, Fig. S3*B*), thereby keeping high-enough cohesin levels remaining required for essential functions during

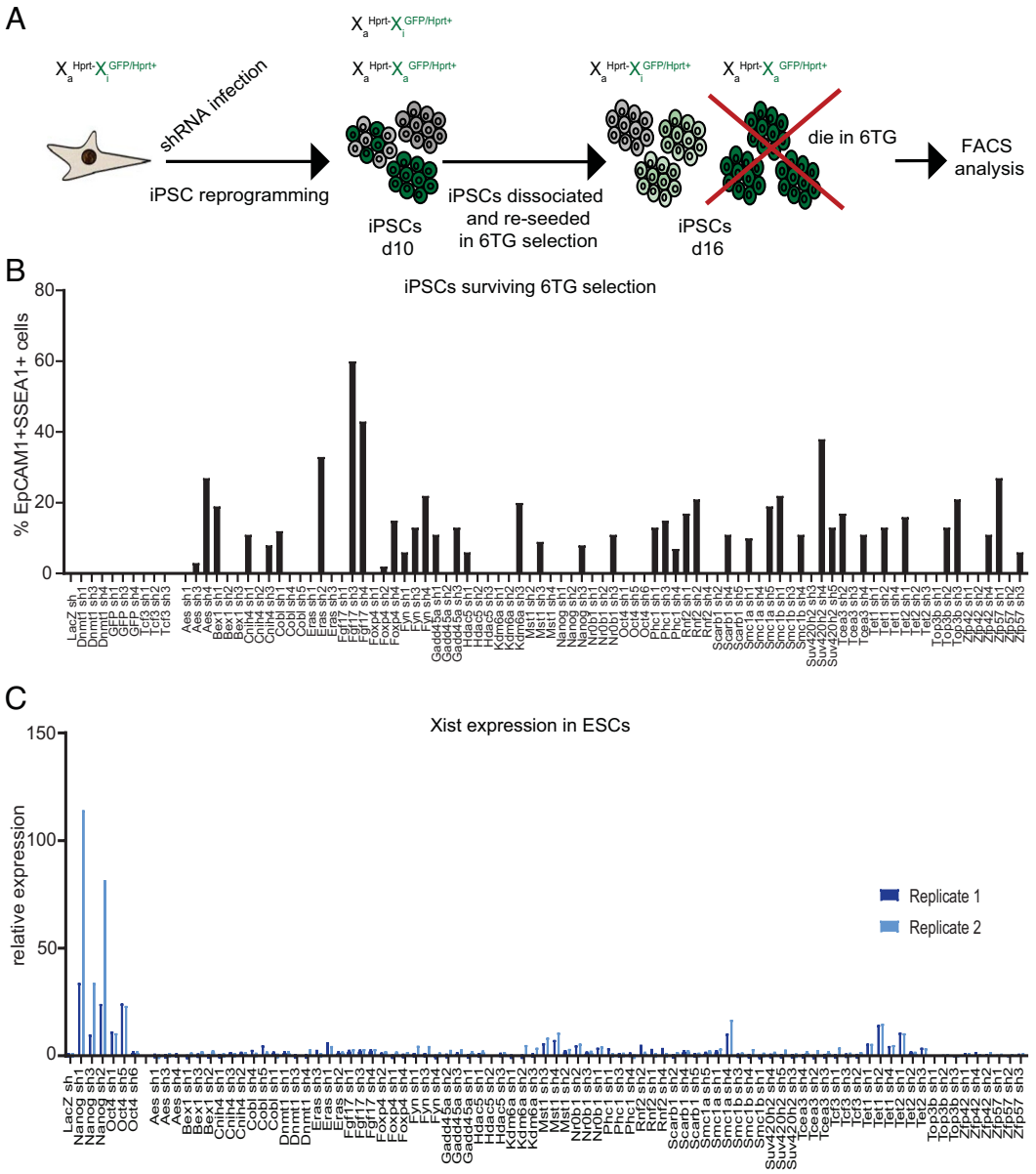

Fig. 2. Impact of candidate knockdown on the reactivation of the endogenous X-linked gene *Hprt* and *Xist* de-repression (*A*) 6TG selection scheme upon knockdown and reprogramming to assess reactivation of the endogenous X-linked gene *Hprt*. On day 10 of reprogramming, iPSCs were dissociated and one-third of the cells has been reseeded on 24-well plate and cultured under 6TG drug selection for 6 d, which would eliminate iPSCs which have undergone XCR and reactivated *Hprt*. (*B*) Percentage of EpCAM1+ SSEA1+ iPSCs surviving 6 d of 6TG selection analyzed by FACS analysis. shRNAs used for knockdown are indicated in the X axis. Control hairpins against LacZ and GFP and for genes whose knockdown enhances XCR (*Dnmt1Tcf3*) are on the *Left*, while candidates with a potential role in XCR are on the *Right*. (*C*) Relative Xist expression upon XCR candidate knockdown in female ESCs (normalized to LacZ shRNA set as 1). Dark and light blue bars indicate two biological replicates. LacZ shRNA control and pluripotency genes Oct4 and Nanog with a known role in repressing *Xist* (22–24), are shown on the *Left* as controls.

cell division (55, 56) and for reprogramming (36–38). In sum, our results led us to conclude that cohesins have a dosage-dependent role for XCR during iPSC reprogramming, whereas the reduction in cohesin levels does not significantly affect the efficiency of pluripotency acquisition. Consequently, as a reduction in XCR did not go hand in hand with a reduction in iPSC colony or cell number suggests that XCR does not influence iPSC-reprogramming efficiency, making them functionally separable events.

SMC1a Is Enriched on the Active X Chromosome, and Its Depletion Leads to the Compaction of the Active X. As SMC1a-depletion had a preferential effect on XCR, this would be in line with the model that cohesins control the 3D-chromatin structure of the active X chromosome and are evicted by Xist RNA from the inactive X (29, 32). Therefore, to understand how SMC1a could play a role in XCR, we focused our attention on X chromosome structure. We performed SR stochastic optical reconstruction microscopy (STORM) (57) in MEF cells in Smc1a knockdown and control conditions. Specifically, we performed immuno-DNA FISH using an X chromosome paint probe to identify the two X chromosomes followed by immunofluorescence for H3K27me3 and SMC1a. This allowed us to discriminate the H3K27me3-enriched inactive Xi from the active Xa and to quantify with single-cell resolution the relative amount of SMC1a protein bound on each X chromosome by STORM imaging (Fig. 4*A*). As expected, control LacZ shRNA MEFs showed an abundant and broadly distributed signal of SMC1a across the nucleus and significant depletion from the Xi when compared with the Xa (Fig. 4 *A* and *B*), in agreement with bulk ChIP-Seq data for SMC1a (29). Due to the higher compaction of the Xi, the density of SMC1a localizations per area did not differ significantly between the Xi and Xa (Fig. 4*C*). Accordingly, there was more

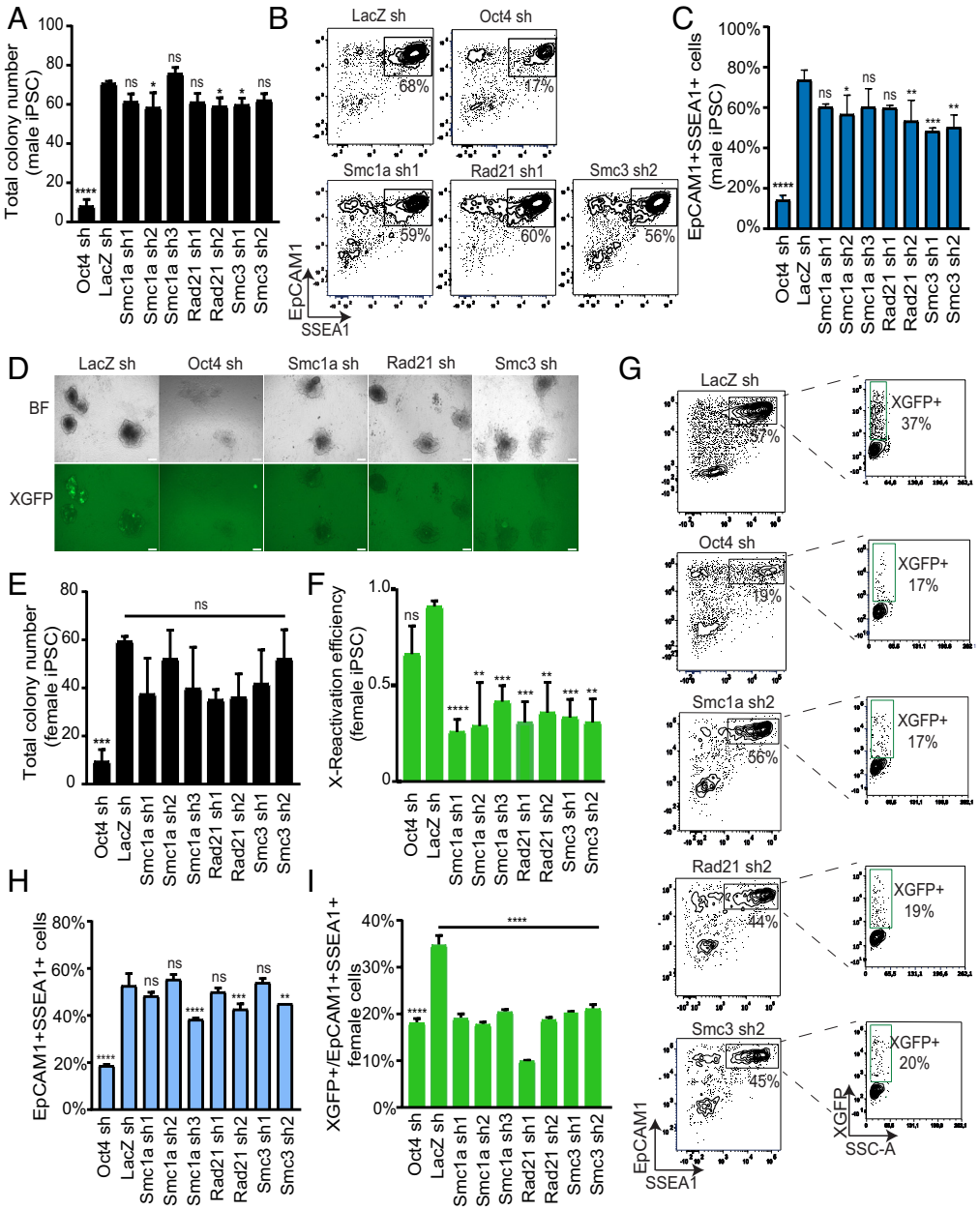

Fig. 3. Cohesin complex members have a preferential role in XCR during iPSC reprogramming. (*A*) Total colony numbers upon cohesin members knockdowns in male cells. (*B*) Flow cytometry analysis of iPSC colonies w/wo cohesin knockdown stained for EpCAM1 and SSEA1 at day 11 of reprogramming in male cells. (*C*) Quantification of double-positive EpCAM1/SSEA1 cells upon cohesin knockdown. (*D*) Representative images of female iPS colonies at day 10 showing the colony formation in brightfield (BF) and the XGFP reactivation upon knockdown in green (Scale bars = 50 μm.) (*E*) Total colony number upon cohesin members' knockdown in female cells. All samples below the horizontal line are not significantly different from lacZ control. (*F*) XCR efficiency scored as ratio between XGFP positive colony number and the total colony number at day 10 upon cohesin members' knockdown in female cells. (*G*) Flow cytometry analysis of iPSC colonies w/wo cohesin knockdown stained by EpCAM1 and SSEA1 at day 11 of the reprogramming in female cells. (*H*) Quantification of double-positive EpCAM1/SSEA1 population in female cells. (*I*) XGFP percentage scored within the pluripotent population (EpCAM1 and SSEA1 double-positive cells). All samples below the horizontal line are significantly different from lacZ control with ****$P \leq 0.0001$. In all panels Oct4 shRNA is shown as reprogramming control. In panels (*A*, *C*, *E*, *F*, *H,* and *I*): Mean ± SD is displayed. Statistical comparisons with control LacZ shRNA controls are indicated. ns $P > 0.05$, *$P \leq 0.05$, **$P \leq 0.01$, ***$P \leq 0.001$, ****$P \leq 0.0001$ for one-way ANOVA with Dunnett's multiple comparisons test, n = 3 replicates.

SMC1a bound on the Xa compared with its respective Xi, when scoring the ratio of SMC1a localizations between the Xa and Xi within the same nucleus (Fig. 4*D*). In Smc1a shRNA MEFs, we detected a drastic reduction of cohesin in the nucleus and STORM imaging confirmed almost complete absence of detectable SMC1a protein, with just few spots remaining (Fig. 4*A*) and leading to the disappearance of the higher amount of bound SMC1a on the Xa when compared with the Xi (Fig. 4 *B* and *D*).

We next asked whether Smc1a knockdown would affect the global organization of X chromosomes. Thus, we measured the area occupied by the active versus inactive X chromosomes in LacZ and Smc1a shRNA conditions. As the heterochromatic Xi is more compact than the Xa (30, 58, 59), the area occupied by the active X was significantly bigger than the area occupied by the Xi in LacZ knockdown controls (Fig. 4 *A*–*E*). On the contrary, upon Smc1a knockdown, the area differences between the two X chromosomes disappeared as the active X area became smaller and more similar to the inactive X (Fig. 4*E*). Surprisingly, when we compared the area occupied by H3K27me3 on the Xi between control LacZ and Smc1a knockdown cells, we observed that the H3K27me3 area was significantly smaller and the H3K27me3 signal appeared more intense after SMC1a depletion (Fig. 4 *F* and *G* and

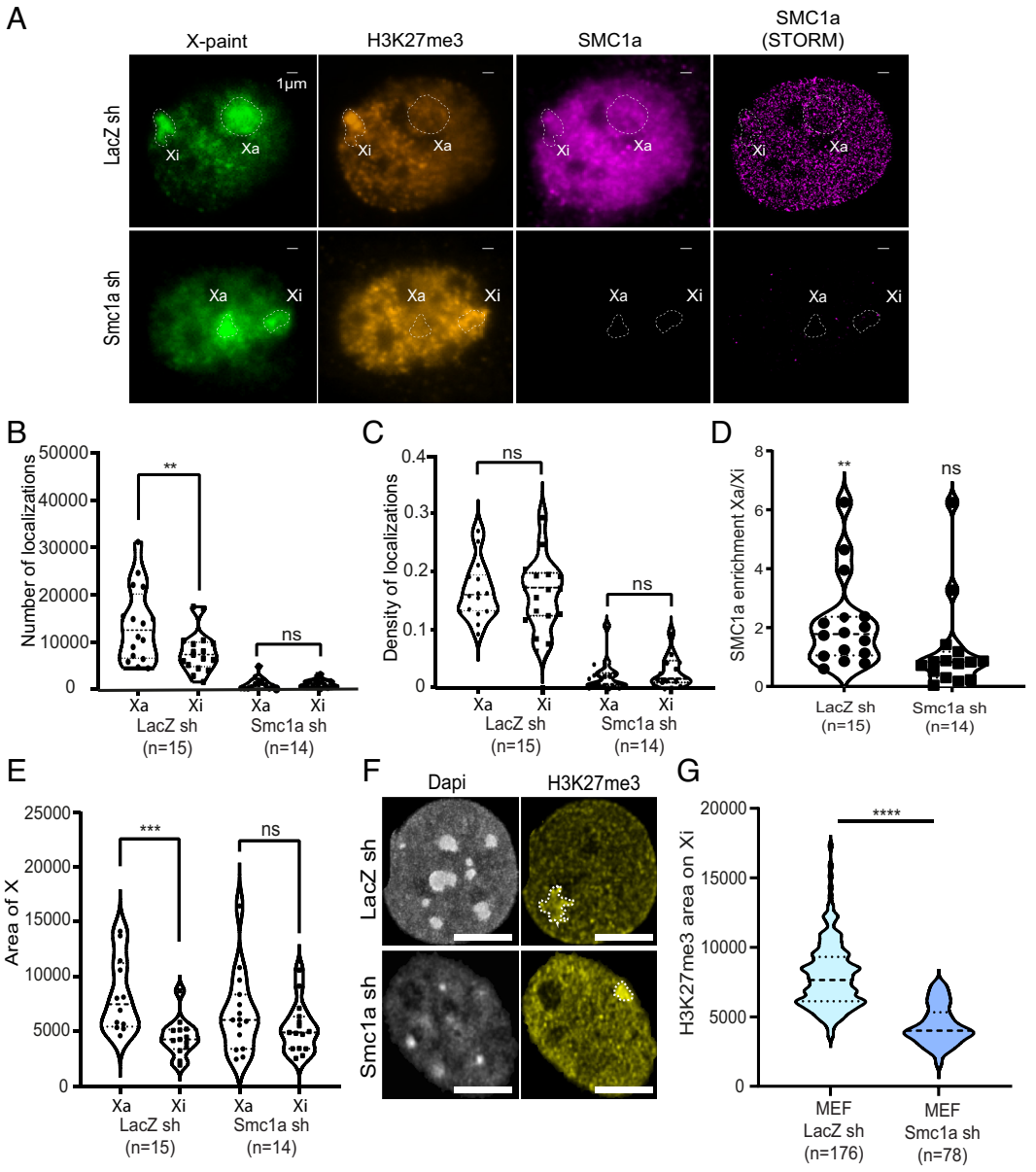

Fig. 4. Differential localization of SMC1a between active and inactive X chromosomes shapes X chromosome territory. (*A*) Representative images of Immuno-DNA FISH experiments in combination with super resolution microscopy (STORM). MEFs with Smc1a or LacZ control shRNA knockdown were stained with X-paint (green), H3K27me3 (orange), and SMC1A (magenta). The dashed areas outline the two X chromosome territories (Xi = inactive X; Xa = active X) (scale bars = 1 μm). Diffraction-limited images for X-paint, H3K27me3 and SMC1a are shown in the left three columns. STORM images of SMC1a are shown in the right column. (*B*) Average number of SMC1a localizations per chromosome in LacZ shRNA control and Smc1a knockdown MEFs for both active and inactive X chromosomes. (Mean ± SD is displayed. $^{**}P \leq 0.01$ for two-tailed paired *t* test). Numbers indicate the absolute number of counted cells. (*C*) Density of SMC1a localizations in LacZ shRNA control and Smc1a knockdown MEFs for both active and inactive X chromosomes. Density was quantified by dividing the number of SMC1a localizations identified in the active and inactive chromosome shown in (*B*) by the area of the corresponding chromosome (Mean ± SD is displayed. ns $P > 0.05$ for two-tailed paired *t* test). Numbers indicate the absolute number of counted cells. (*D*) Ratio of SMC1a localizations in Xa/Xi per nucleus. (Mean ± SD is displayed. $^{**}P \leq 0.01$ for one sample *t* test). Numbers indicate the absolute number of counted cells. (*E*) Quantification of the active and inactive X chromosome areas after control LacZ (*Left*) and Smc1a (*Right*) shRNA knockdown in MEFs. (Mean ± SD is displayed. $^{***}P \leq 0.001$ for two-tailed paired *t* test). Numbers indicate the absolute number of counted cells. (*F*) Representative confocal images of H3K27me3 mark upon LacZ and Smc1a shRNA knockdown in MEFs. The dashes areas outline the H3K27me3 spot (Scale bars = 9 μm.) (*G*) Comparison of inactive X chromosomal H3K27me3 territory after LacZ and Smc1a shRNA knockdown. ($^{****}P \leq 0.0001$ for unpaired *t* test). Numbers indicate the absolute number of counted cells.

SI Appendix, Fig. S4), although the Xi area based on X-paint did not change (Fig. 4*E*). This suggests a potential role for SMC1a in defining the H3K27me3 territory on the Xi.

Taken together, our data showed an increase in compaction upon Smc1a knockdown on the active X, suggesting a function for SMC1a in shaping the Xa structure. Furthermore, we observed a contraction of the H3K27me3 territory on the Xi without changing the overall Xi-chromosome compaction after Smc1a knockdown, highlighting distinct roles for SMC1a on the active and inactive X chromosomes (32).

X Chromosome Architecture Is Rewired during Pluripotency Acquisition in an SMC1a-Dependent Fashion. To interrogate the cohesin dependency of the dynamic structural changes of the X chromosomes during iPSC reprogramming, we used a combined oligopaint and immunolabeling approach similar to (30). As depicted in the cartoon in Fig. 5*A* and *SI Appendix*, Fig. S5*A*, we designed DNA-FISH probe sets according to the megadomain structure characteristically present on the Xi but not on the Xa (27–30). Analysis of published Hi-C data (21) revealed that the probe sets were each separated by approximately

5 to 10 TADs (topologically associating domains) on the Xa and that they localized in different compartments depending on cell type and X-inactivation state (*SI Appendix*, Fig. S5*A*). Specifically, we designed the probes within the left megadomain (probe sets a, b) and in the right megadomain (probe set c) divided into two subregions within each area (a1–a2, b1–b2, c1–c2). This allowed us to measure 3D-distances both within a megadomain (a–b), as well as across the megadomain boundary *Dxz4* (probes b–c). We used these probes to examine intra- and intermegadomain distances on both the active and inactive X chromosomes in three different cell states: MEFs (differentiated XaXi state), day 8 iPSCs (intermediate reprogramming XaXi to XaXa state) and ESCs (pluripotent XaXa state) (Fig. 5*B* and *SI Appendix*, Fig. S5*B*).

First, we observed a progressive increase in both (a-b) as well as (b-c) distances on the Xa, when comparing differentiated MEFs, day 8 reprogramming intermediates and pluripotent ESCs, which is in line with a globally decompacted chromatin state in pluripotent cells in contrast to differentiated cells (60, 61) (Fig. 5*B* and *SI Appendix*, Fig. S5*B*). Next we compared probe distances on the Xi with the distances on the Xa in differentiated cells (MEFs) and observed relatively small, but significant differences between probes (a-b), consistent with them being located within one compacted megadomain on the Xi and the megadomain-free, more open Xa (Fig. 5 *C* and *D*). Upon Smc1a knockdown, this difference was lost (Fig. 5*C* and *SI Appendix*, Fig. S5*C*), in line with our results when comparing the Xi and Xa compaction states using X-paint (Fig. 4*E*), and also consistent with the loss of megadomains on the Xi after cohesin depletion (32). We then went on to examine day 8 of reprogramming, as this is the time point when XCR starts to occur in this system, allowing us to differentiate between the inactive X from the active or reactivated X by the presence or absence/loss of the H3K27me3 spot, respectively (Fig. 5 *E* and *F*). We did not observe significant differences in the distances spanning the megadomains (probes b–c) between Xa and Xi consistent with a previous study (30). However, when comparing intra-megadomain distances (a–b), we saw a significant distance increase on the Xa, once the H3K27me3 spot has been erased during XCR (XaXa cells), but not prior to XCR (XaXi cells). This suggests that progression in reprogramming and XCR promoted the restructuring of both the constitutively active Xa as well as the freshly reactivated Xa. Finally, we wanted to see how cohesin affected the structure of the Xa in ESCs (Fig. 5 *G* and *H*). Compared with LacZ knockdown control, after Smc1a knockdown (*SI Appendix*, Fig. S5*D*) we saw a marked reduction in b–c probe distances and to some, but nonsignificant degree, of a–b probe distances. This decrease in probe distances upon Smc1a knockdown indicated a transition toward a distinct Xa structure when cohesin levels were reduced. This is in agreement with what we have observed for the Xa in MEFs after Smc1a depletion (Figs. 4*E* and 5 *C* and *D*).

In conclusion, the X chromosome displays progressive reorganization during reprogramming, both when reactivated from an Xi to an Xa and when transitioning as Xa from a differentiated to a pluripotent cell state. The cohesin SMC1a appears to be a key factor during this process as its depletion leads in particular to a collapse of the Xa structure.

Discussion

Reactivation of the inactive X chromosome in females is a hallmark of the naive pluripotent stem cell state (4–6) and occurs in the mouse blastocyst epiblast in vivo (7) and during iPSC reprogramming in vitro (18). While a number of studies have described the sequence of events (9, 10, 19–21, 25), little is known about the factors driving this chromosome-wide epigenetic reprogramming process. To gain mechanistic insight, we here went on to perform a candidate-based RNAi-knockdown screen during iPSC-reprogramming to uncover regulators of XCR.

The main hit from our screen, which we followed up mechanistically, was the cohesin complex member SMC1a (35, 54). SMC1a has caught particularly our attention, as it has been described to be evicted from the inactive X chromosome by Xist RNA during X-inactivation (29, 32). This leads to the characteristic structural differences between the Xi and Xa, where the Xi loses most of its topological domains (29, 30). The structures are regained after conditional ablation of Xist in fibroblasts (29) or during iPSC-reprogramming, when Xist is down-regulated and the Xi is remodeled into an Xa by XCR (21). Previous studies focused on the role of cohesin for X chromosome structure in the context of X-inactivation establishment during differentiation and during X-inactivation maintenance (29, 32). What sets our study apart is that our goal was to elucidate the importance of cohesin in setting up and remodeling the Xa structure during the reverse process of XCR and pluripotency acquisition. Furthermore, instead of using a bulk, genomics-based approach, we chose a combination of super resolution (STORM) and conventional imaging, in order to resolve the cell-to-cell heterogeneity occurring during the dynamic reprogramming process.

We selected a number of our candidates based on their expression in mouse blastocysts, where they got up-regulated during epiblast maturation between E3.5 and E4.5 and thereby anticorrelated with *Xist*, which gets down-regulated during XCR. We hypothesized that low expression in pre-XCR epiblast and increase in expression during XCR would enrich for factors with a potential active role in XCR. Despite the anticorrelation of many of our candidates with *Xist* expression, we did not uncover new regulators of *Xist*, which is known to be repressed by pluripotency factors such as OCT4, NANOG, and PRDM14 (9, 22–24), as the knockdown of our candidates in ESC did not lead to *Xist* derepression. Instead, our screen led us to identify a number of factors, which, when knocked down during iPSC-reprogramming, either resulted in reduced overall reprogramming efficiency and/or in fewer cells undergoing XCR through *Xist* regulation-independent mechanisms. While it was expected that genes that affect iPSC-reprogramming would also indirectly impact XCR efficiency, it was not known if the opposite holds true. In particular, there is an intricate feedback between X-inactivation and pluripotency exit, where dosage-sensitive X-linked genes need to be silenced by X-inactivation in order to promote ESCs to differentiate (62–64). The fact that we discovered genes like cohesins, whose knockdown would impair XCR without at the same time affecting iPSC-reprogramming efficiency speaks at a first glance against a model, where XCR would be required for generating iPSCs. It rather suggests that iPSC-reprogramming and XCR are to some degree functionally separable processes. This can be explained by XCR being a relatively late reprogramming event (65), which occurs after early events such as expression of the pluripotency cell surface markers SSEA1 and EpCAM1 (50) and mesenchymal-to-epithelial transition (66, 67) leading to iPSC colony formation, which we used as our readouts for iPSC-reprogramming efficiency. Nevertheless, we still expect XCR to influence final iPSC quality, specifically when it comes to global DNA-methylation levels and MAPK-signaling, which are regulated by X chromosome dosage (62–64, 68, 69). Furthermore, XCR requires *Xist* downregulation (10, 19), which is controlled by pluripotency factor expression during iPSC-reprogramming (9, 22–24). This indicates that overall, XCR and pluripotency acquisition are tightly coupled during different phases of the iPSC-reprogramming process.

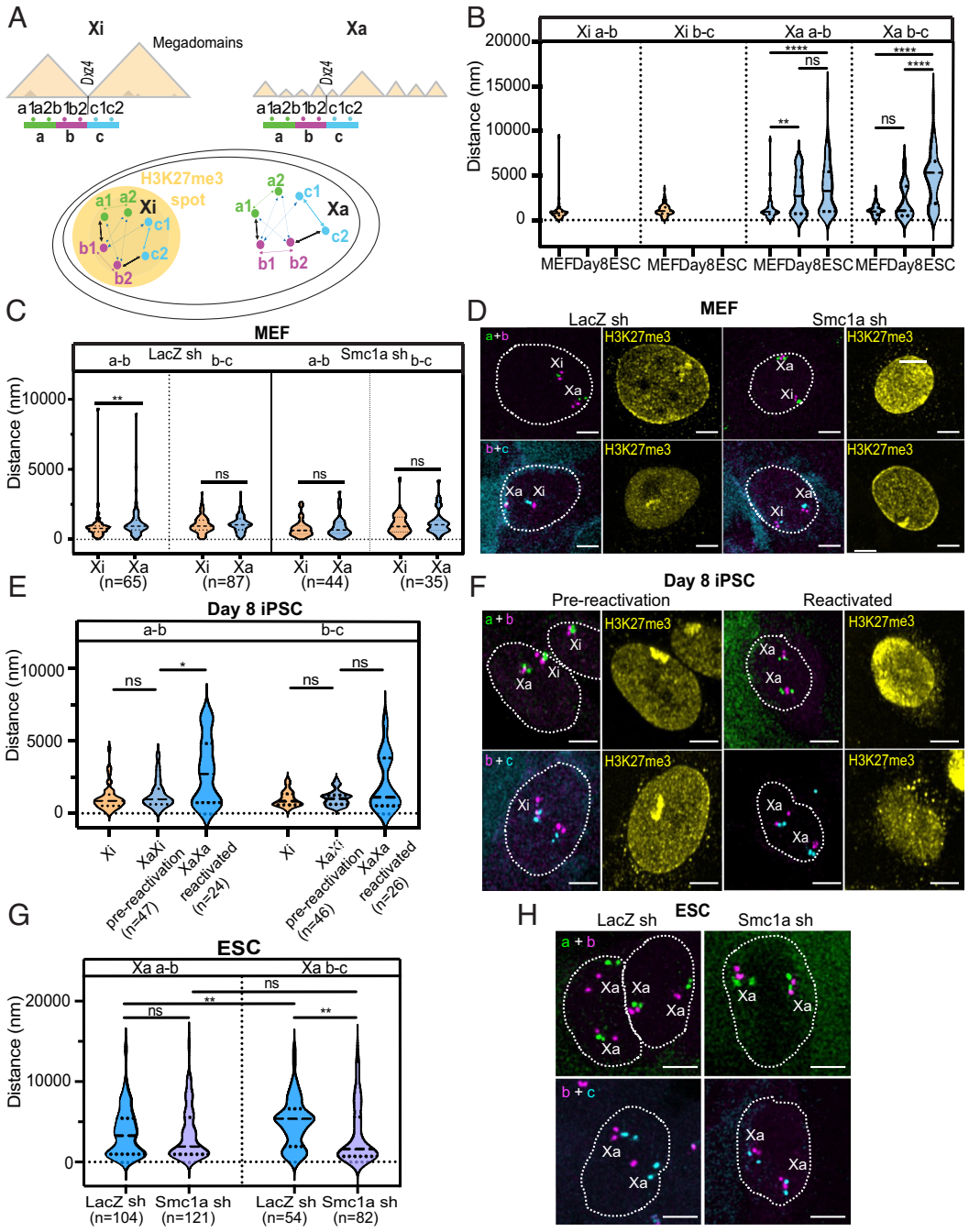

Fig. 5. Remodeling of intra- and intermegadomain distances on the active and inactive X chromosomes during iPSC reprogramming. (*A*) Diagram of the experimental setup using oligopaint probes for regions a, b (*Left* megadomain) and c (*Right* megadomain). Within each region, two subregions were labeled and detected (a1, a2, b1, b2, c1, and c2), the distances between subregions were scored and the shortest distances between probes of different subregions (bold black arrows) selected as a–b and b–c distances. (see *SI Appendix*, Fig. S5*A* for probe location in relation to TADs and compartments). (*B*) Violin plots of the shortest distances between a–b and b–c megadomains in LacZ control knockdown MEFs, day 8 of reprogramming and ESCs labeled with oligopaint probes. The shortest distances measured for each locus are plotted. Oligopaint signals belonging to Xa and Xi were classified based by the overlap with the H3K27me3-rich signal accumulated on the Xi (see *SI Appendix*, Fig. S5*B* for representative examples). Median ± IQR is displayed. ns $P > 0.05$, ****$P \leq 0.0001$ for two-tailed unpaired *t* test. Numbers indicate the absolute number of counted cells. (*C*) Violin plots of the distances between a–b and b–c mega domains in LacZ-control and Smc1a-shRNA MEFs, labeled with oligopaint probes. The shortest distances measured for each loci are plotted. Oligopaints signals belonging to Xa and Xi were classified based on the overlap with the H3K27me3-rich signal accumulated on the Xi. Median ± IQR is displayed. ns $P > 0.05$, **$P \leq 0.01$, for two-tailed unpaired *t* test. Numbers indicate the absolute number of counted cells. (*D*) Representative confocal images (maximum intensity projections) of LacZ- and Smc1a-shRNA MEFs, labeled with oligopaint probes for regions a (AF488, in green), b (AF647, in magenta) and c (AF488, pseudocolored in cyan). Nuclear areas are shown with a dashed line, Xa and Xi were classified based on the overlap with H3K27me3-rich signal accumulated on the Xi (AF568, in yellow) (Scale bars = 5 μm.) (*E*) Violin plots of the distances between a–b and b–c mega domains in LacZ-control cells at day 8 of reprogramming, labeled with oligopaint probes. The shortest distances measured for each loci are plotted. Oligopaints signals belonging to Xa and Xi were classified based on the overlap with the H3K27me3-rich signal accumulated on the Xi, which is present in XaXi prereactivation cells and absent in XaXa reactivated cells. Median ± IQR is displayed. ns $P > 0.05$, *$P \leq 0.05$, for two-tailed unpaired *t* test. Numbers indicate the absolute number of counted cells. (*F*) Representative confocal images (maximum intensity projections) of LacZ-control cells at day 8 of reprogramming labeled with Oligopaint probes for regions A (AF488, in green), B (AF647, in magenta) and C (AF488, pseudocolored in cyan). Nuclear areas are shown with a dashed line, Xa and Xi were classified based on the overlap with H3K27me3-rich signal accumulated on the Xi (AF568, in yellow) (Scale bars = 5 μm.) (*G*) Violin plots of the distances between a–b and b–c mega domains in LacZ-control and Smc1a-shRNA ESCs, labeled with oligopaint probes. The shortest distances measured for each loci are plotted. Median ± IQR is displayed. ns $P > 0.05$, **$P \leq 0.01$, for two-tailed unpaired *t* test. Numbers indicate the absolute number of counted cells. (*H*) Representative confocal images (maximum intensity projections) of LacZ-control and Smc1a-shRNA ESCs labeled with oligopaint probes for regions a (AF488, in green), b (AF647, in magenta), and c (AF488, pseudocolored in cyan). (Scale bars = 5 μm.)

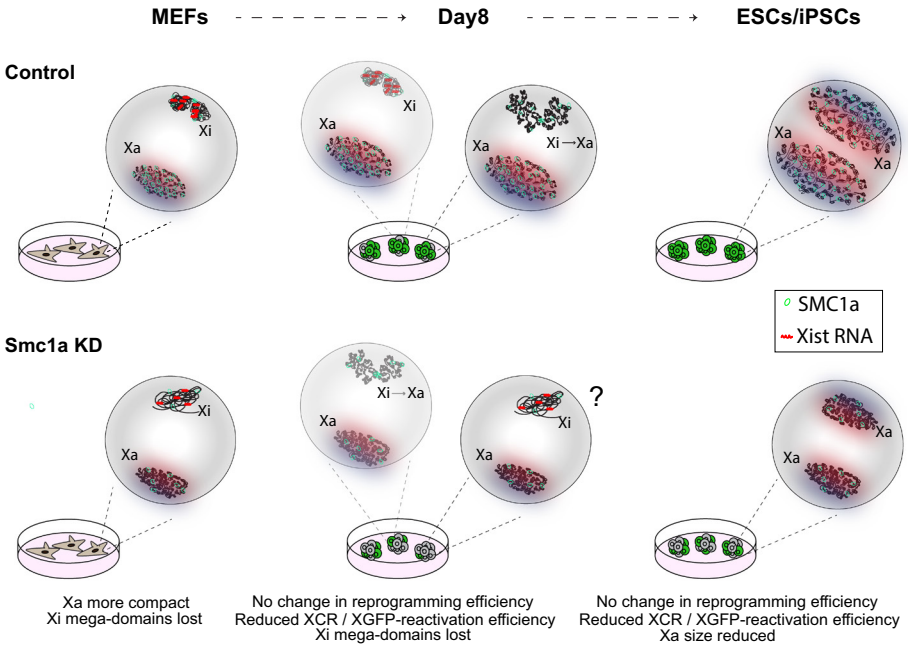

Fig. 6. Schematic representation of the proposed model for SMC1a function in the remodeling of the X chromosomes and XCR during iPSC-reprogramming. Under control conditions (*Top*), MEFs have an Xa, which is larger in volume and bound by more SMC1a protein (green circles), than the Xi, where Xist RNA coating repels SMC1a, leading to a more compact structure. Upon Smc1a knockdown (KD, *Bottom*), the Xi loses its megadomain structure (as shown in ref. 32), while the Xa becomes more compact (this study). On day 8 of iPSC-reprogramming, wt cells are undergoing XCR and reactivating XGFP. Some cells still contain an Xist-coated/H3K27me3 enriched Xi and an Xa (shaded, prereactivation), and some cells contain an Xa and an Xi on the path to becoming an Xa (Xi→ Xa) by having lost Xist coating/H3K27me3 enrichment (reactivated). Smc1a knockdown cells form iPSC colonies at similar rates to controls, but do not undergo XCR and reactivate XGFP as efficiently. The ? indicates that we did not assess the X chromosome structure in KD cells on day 8 and therefore can only speculate about it at this time point. At the end of reprogramming, wt iPSC colonies become mostly XGFP+, i.e., completion of XCR. In pluripotent stem cells (ESCs and iPSCS), the two Xa chromosomes reach their most relaxed state. Smc1a KD perturbs XCR/XGFP-reactivation in iPSCs and leads to restructuring of the Xa chromosomes in ESCs.

Our observation that cohesin knockdown did not interfere with iPSC-reprogramming initially surprised us considering the importance of cohesin for many essential cellular functions during cell cycle and genome regulation (35, 54, 55). Previous studies reported a role for cohesin in enabling long-range genomic interactions, which promote the expression of pluripotency genes such as *Nanog* and *OCT4* and in turn would affect iPSC-reprogramming efficiency (36) or pluripotency maintenance (37, 38). However, studies based on reprogramming by cell fusion of differentiated cells with pluripotent stem cells in the absence of cell proliferation reported that cohesins were not essential for pluripotency gene expression, but rather played a role during cell cycle progression and genome stability (39, 40). As in our knockdown experiments cohesins were depleted only partially (with about 17 to 35% remaining at the RNA-level), this would leave high-enough amounts for essential cohesin functions during cell proliferation and pluripotency gene regulation intact without impacting iPSC reprogramming efficiency.

On the contrary, XCR and X chromosome structure were highly sensitive to the reduction in cohesin dosage during knockdown in our system (Fig. 6), in line with the key role cohesin plays for X chromosome structure and activity (29, 32). All cohesins we tested—SMC1a, RAD21 and SMC3—showed an almost identical reduction in XCR after knockdown, in accordance with their essential function for the cohesin complex (35, 54, 70). While *Xist* regulation seems not to be the main mechanism by which cohesins control XCR, it rather acts by modulating X chromosome structure. The Xi structure is characterized by an attenuation of loops/topological domains and separation of the chromosome into two megadomains, while the Xa retains loops and topological domains but does not acquire megadomains (29, 30). Using STORM SR microscopy, we observed that SMC1a was enriched on the Xa when compared with the Xi at the individual nucleus level—thereby confirming what has been reported previously by bulk ChIP-seq analysis (29, 32). We found that the Xa, which is normally less compacted than the Xi, became more compact after Smc1a knockdown thereby erasing differences in X-area and intra-chromosomal distances between the Xa and Xi in MEFs. A similar effect of cohesin depletion has been also reported for autosomes during mitosis (71), where cohesins were replaced after knockdown by RB and condensin leading to hypercompaction of mitotic chromosomes. Future studies should clarify, if similar events involving other factors could be also the mechanism responsible for the compaction of the Xa after Smc1a knockdown in interphase. Furthermore, it will be of interest to directly compare side-by-side the effect of cohesin depletion on the Xa with autosomes in order to discriminate between Xa-specific and general effects.

In contrast to the compaction effect on the Xa in MEFs when depleting SMC1a, we observed no major changes to the overall size of the already compact Xi in the same cell. However, what we did see was a substantial reduction in the H3K27me3 territory on the Xi. Instead of covering the entire Xi territory as in controls, Smc1a knockdown led to shrinkage of the H3K27me3 area concomitantly with intensification of the H3K27me3 signal within the chromosomal territory defined by X chromosome paint. It has been shown previously that the bipartite megadomain structure characteristic for the Xi (27–30) collapses after cohesin depletion (32). In turn this might lead to enhanced compaction of the Polycomb compartment, as compartment structures in general (72–75) and Polycomb-mediated interactions in particular (76, 77) are counteracted by cohesin and strengthened in its absence. As the Xi contains an underlying compartmentalization based on different chromatin types (H3K27me3 vs. H3K9me2/3-based heterochromatin) (21, 33, 78), self-association of the Polycomb compartment on the Xi by phase separation, a feature of Xi chromatin (79–81), could be enhanced when cohesin is depleted. Although this phenomenon will need further examination,

it could potentially explain our observation of H3K27me3-domain size reduction on the Xi after Smc1a knockdown. It would be interesting to investigate in future studies the effects of cohesin depletion on the distribution of H3K27me3 across the Xi and how this in turn may affect gene reactivation during reprogramming.

When we used Oligopaints to measure distances within and across megadomain regions during reprogramming, we found an increase in probe distances when the Xi has been reactivated, but even a greater, progressive increase in distances on the Xa when cells became pluripotent, consistent with a generally more relaxed chromatin state associated with pluripotency (60, 61) (Fig. 6). Like in MEFs, Smc1a knockdown in ESCs led to restructuring of the active X chromosomes, indicating that cohesin has important functions in shaping the Xa structure in both pluripotent and differentiated cells. As our current study examined the impact of cohesin depletion on X-structure in ESCs as pluripotent cell type but not directly in iPSCs, further analysis will be needed to confirm if the effects are equivalent or if differences exist.

What still remains open is how cohesin facilitates reactivation of X-linked genes during XCR, as cohesin can regulate chromatin structure and gene expression at multiple levels (35). Loops and topological domains are absent/strongly attenuated on the Xi (30, 31) due to Xist repelling cohesin and CTCF (29, 32) and are reestablished with XCR during iPSC-reprogramming (21). In our previous work, we have found that the kinetics of TAD formation is not predictive of gene reactivation (21). Specifically, we found that TAD formation mostly precedes transcriptional reactivation and is therefore not dependent on it. Furthermore, we did not see any correlation between early forming TADs and early reactivating genes, which made us conclude that TAD formation and transcriptional reactivation are unlikely to be causally linked. Therefore, we believe that cohesin plays a TAD-independent role in gene reactivation during XCR, while leaving open the role of cohesins in reestablishing functional loops and other topological domains. Even while cohesin or CTCF depletion has only a modest impact on gene expression in the steady cell state (72, 82), another possibility is that cohesin could promote specific enhancer/promoter interactions switching silent genes to an active state during XCR. Finally, XCR involves global chromatin changes such as the erasure of the polycomb-mediated H3K27me3 mark (7, 10, 13). Cohesin is known to counteract chromatin compartmentalization (72–75) and in particular disrupt polycomb-mediated compartments (76, 77). Therefore, rebinding of cohesin to the Xi after Xist downregulation might facilitate the conversion of the polycomb/H3K27me3-rich facultative heterochromatin compartment into a transcriptionally permissive euchromatic A-compartment. A limitation of our present study is that we used *XGFP* and *Hprt* as proxies for X-linked gene reactivation. Therefore, we do not know if all X-linked genes rely equally on cohesin for their reactivation and to which extent the location in different chromatin environments might affect cohesin dependency. Further studies will need to clarify the exact mechanism of action of cohesin during XCR.

Overall, our study identifies the cohesin complex member SMC1a as a key factor involved in X chromosome structural changes and XCR during iPSC-reprogramming. We provide evidence that cohesin-mediated chromosome architecture remodeling plays an important role in switching the X chromosome from an inactive to an active state without impacting overall iPSC-reprogramming efficiency. We thereby demonstrate context-dependent and chromosome-specific functions for cohesin and provide the basis for further studies on the role of chromatin structure in transcriptional regulation.

Material and Methods

The information on mouse cell lines and culture conditions used in this study is provided in *SI Appendix*. List of candidate genes is available in *SI Appendix*, Table S1. Detailed experimental methods about iPSC induction, cell infection, RNA extraction, quantitative PCR, flow cytometry, immunofluorescence, and combined Oligopaint and immune labeling are also provided in the extended supporting information. Primers for qPCR analysis are listed in Dataset S4. Antibodies used in this study are listed in Dataset S5. Oligo sequences used to amplify and detect Oligopaint probes are provided in Dataset S6. shRNA information is listed in Dataset S7.

Data, Materials, and Software Availability. All study data are included in the article and/or supporting information. Previously published data were used for this work (GEO data series GSE208430, GSE4307).

ACKNOWLEDGMENTS. We are grateful to present and previous J.T.L. and B.P. lab members for discussions and input. We further thank P. Kharchenko and P. Park for help in the initial single-cell analysis. We thank former members of the K.H. lab, in particular M. Stadtfeld, E. Apostolou, N. Maherali, M. Borkent, and S. Cheloufi for help with establishing iPSC-reprogramming conditions. We acknowledge critical technical support by the CRG core facilities including the CRG/UPF FACS Unit; the Advanced Light Microscopy Unit (ALMU) and the PRBB Animal Facility. We especially thank R. Gomez Riera (ALMU) for developing the macros for nuclear segmentation and scripts for measuring loci distances. This work was supported by the Spanish Agencia Estatal de Investigación (AEI) of the Ministry of Science and Innovation (PID2020-114080GB-I00 and BFU2017-86760-P (AEI/FEDER, UE) to M.P.C.; and BFU2014-55275-P, BFU2017-88407-P, EUR2019-103817, PID2021-123383NB-I00 to B.P.), the AXA Research Fund (to B.P.) and the Agencia de Gestio d'Ajuts Universitaris i de Recerca (AGAUR, 2017 SGR 689 to M.P.C. and 2017 SGR 346 to B.P.). M.P.C. is supported by ICREA (Institucio Catalana de Recerca i Estudis Avançats). We would like to thank the Spanish Ministry of Economy, Industry and Competitiveness (MEIC) to the EMBL partnership and to the "Centro de Excelencia Severo Ochoa". We also acknowledge support of the CERCA Programme of the Generalitat de Catalunya. M.V.N. has been supported by the People Program (Marie Curie Actions) FP7/2007–2013 under REA grant [608959] from the European Union and a Juan de la Cierva-Incorporación 2017 from the Spanish Ministry of Science and Innovation. P.A. has received funding from the European Union's Horizon 2020 research and innovation program under the Marie Skłodowska-Curie grant agreement No 747488. M.B. has been supported by an EMBO postdoctoral fellowship (ALTF682–2021). J.T.L. is supported by the U.S. NIH grant, R01-MH118351. Portions of this work have appeared as part of the PhD dissertation "Screen for novel factors involved in pluripotency and X chromosome reactivation." by S.F.G. (Universitat Pompeu Fabra, 2019).

Author affiliations: [a]Centre for Genomic Regulation, The Barcelona Institute of Science and Technology, Barcelona 08003, Spain; [b]Department of Genome Sciences, University of Washington, Seattle, WA 98195; [c]Department of Molecular Biology, Massachusetts General Hospital, Boston, MA 02114; [d]Department of Pathology, Massachusetts General Hospital, Boston, MA 02115; [e]Institute for the Advanced Study of Human Biology, Kyoto University, Kyoto 606-8501, Japan; [f]Department of Anatomy and Cell Biology, Graduate School of Medicine, Kyoto University, Kyoto 606-8501, Japan; [g]Center for iPS Cell Research and Application, Kyoto University, Kyoto 606-8507, Japan; [h]Oncode Institute, Hubrecht Institute, Royal Netherlands Academy of Arts and Sciences and University Medical Center Utrecht, Utrecht 3584, The Netherlands; [i]Cancer Center and Center for Regenerative Medicine, Massachusetts General Hospital, Boston, MA 02114; [j]Universitat Pompeu Fabra, Barcelona 08003, Spain; [k]Institució Catalana de Recerca i Estudis Avançats, Barcelona, 08010 Spain; and [l]Department of Genetics, The Blavatnik Institute Harvard Medical School, Boston, MA 02114

Author contributions: S.F.G., M.V.N., J.T.L., and B.P. conceived the study and designed research; S.F.G., M.V.N., K.K., Y.Y., R.R., M.B., and B.P. performed research; E.A.H., K.H., and B.J.B. contributed new reagents/analytic tools; S.F.G., M.V.N., R.I.S., M.B., J.T.L., and B.P. analyzed data; M.S., M.P.C., J.T.L., and B.P. supervised the work; and S.F.G., M.V.N., P.A., and B.P. wrote the paper with input from the other authors.

1. M. F. Lyon, Gene action in the X-chromosome of the mouse (Mus musculus L.). *Nature* **190**, 372–373 (1961).
2. B. Payer, J. T. Lee, X chromosome dosage compensation: How mammals keep the balance. *Annu. Rev. Genet.* **42**, 733–772 (2008).
3. F. Dossin, E. Heard, The molecular and nuclear dynamics of X-chromosome inactivation. *Cold Spring Harb. Perspect. Biol.* **14**, a040196 (2022).
4. B. Payer, Developmental regulation of X-chromosome inactivation. *Semin. Cell Dev. Biol.* **56**, 88–99 (2016).
5. A. Panda, J. J. Zylicz, V. Pasque, New insights into x-chromosome reactivation during reprogramming to pluripotency. *Cells* **9**, 2706 (2020).
6. A. Spaziano, D. I. Cantone, X-chromosome reactivation: A concise review. *Biochem. Soc. Trans.* **49**, 2797–2805 (2021).

7. W. Mak *et al.*, Reactivation of the paternal X chromosome in early mouse embryos. *Science* **303**, 666–669 (2004).
8. I. Okamoto, A. P. Otte, C. D. Allis, D. Reinberg, E. Heard, Epigenetic dynamics of imprinted X inactivation during early mouse development. *Science* **303**, 644–649 (2004).
9. B. Payer *et al.*, Tsix RNA and the germline factor, PRDM14, link X reactivation and stem cell reprogramming. *Mol. Cell* **52**, 805–818 (2013).
10. M. Borensztein *et al.*, Contribution of epigenetic landscapes and transcription factors to X-chromosome reactivation in the inner cell mass. *Nat. Commun.* **8**, 1297 (2017).
11. M. Sugimoto, K. Abe, X chromosome reactivation initiates in nascent primordial germ cells in mice. *PLoS Genet.* **3**, e116 (2007).
12. S. M. Chuva de Sousa Lopes *et al.*, X chromosome activity in mouse XX primordial germ cells. *PLoS Genet.* **4**, e30 (2008).
13. A. Mallol, M. Guirola, B. Payer, PRDM14 controls X-chromosomal and global epigenetic reprogramming of H3K27me3 in migrating mouse primordial germ cells. *Epigenet. Chromatin* **12**, 38 (2019).
14. J. Severino *et al.*, Controlled X-chromosome dynamics defines meiotic potential of female mouse in vitro germ cells. *EMBO J.* **41**, e109457 (2022).
15. J. Silva *et al.*, Nanog is the gateway to the pluripotent ground state. *Cell* **138**, 722–737 (2009).
16. I. Cantone *et al.*, Ordered chromatin changes and human X chromosome reactivation by cell fusion-mediated pluripotent reprogramming. *Nat. Commun.* **7**, 12354 (2016).
17. I. Cantone, Reversal of X chromosome inactivation: Lessons from pluripotent reprogramming of mouse and human somatic cells. *J. Translat. Genet. Genom.* **1**, 1–14 (2017).
18. N. Maherali *et al.*, Directly reprogrammed fibroblasts show global epigenetic remodeling and widespread tissue contribution. *Cell Stem Cell* **1**, 55–70 (2007).
19. V. Pasque *et al.*, X chromosome reactivation dynamics reveal stages of reprogramming to pluripotency. *Cell* **159**, 1681–1697 (2014).
20. A. Janiszewski *et al.*, Dynamic reversal of random X-chromosome inactivation during iPSC reprogramming. *Genome. Res.* **29**, 1659–1672 (2019).
21. M. Bauer *et al.*, Chromosome compartments on the inactive X guide TAD formation independently of transcription during X-reactivation. *Nat. Commun.* **12**, 3499 (2021).
22. P. Navarro *et al.*, Molecular coupling of Xist regulation and pluripotency. *Science* **321**, 1693–1695 (2008).
23. M. E. Donohoe, S. S. Silva, S. F. Pinter, N. Xu, J. T. Lee, The pluripotency factor Oct4 interacts with Ctcf and also controls X-chromosome pairing and counting. *Nature* **460**, 128–132 (2009).
24. P. Navarro, M. Moffat, N. P. Mullin, I. Chambers, The X-inactivation trans-activator Rnf12 is negatively regulated by pluripotency factors in embryonic stem cells. *Hum. Genet.* **130**, 255–264 (2011).
25. I. Talon *et al.*, Enhanced chromatin accessibility contributes to X chromosome dosage compensation in mammals. *Genome Biol.* **22**, 1–36 (2021).
26. G. Csankovszki, A. Nagy, R. Jaenisch, Synergism of Xist RNA, DNA methylation, and histone hypoacetylation in maintaining X chromosome inactivation. *J. Cell Biol.* **153**, 773–784 (2001).
27. S. S. P. Rao *et al.*, A 3D map of the human genome at kilobase resolution reveals principles of chromatin looping. *Cell* **159**, 1665–1680 (2014).
28. X. Deng *et al.*, Bipartite structure of the inactive mouse X chromosome. *Genome Biol.* **16**, 152 (2015).
29. A. Minajigi *et al.*, Chromosomes. A comprehensive Xist interactome reveals cohesin repulsion and an RNA-directed chromosome conformation. *Science* **349**, aab2276 (2015).
30. L. Giorgetti *et al.*, Structural organization of the inactive X chromosome in the mouse. *Nature* **535**, 575–579 (2016).
31. C.-Y. Wang, T. Jégu, H.-P. Chu, H. J. Oh, J. T. Lee, SMCHD1 merges chromosome compartments and assists formation of super-structures on the inactive X. *Cell* **174**, 406–421.e25 (2018).
32. A. J. Kriz, D. Colognori, H. Sunwoo, B. Nabet, J. T. Lee, Balancing cohesin eviction and retention prevents aberrant chromosomal interactions, Polycomb-mediated repression, and X-inactivation. *Mol. Cell* **81**, 1970–1987.e9 (2021).
33. E. M. Darrow *et al.*, Deletion of DXZ4 on the human inactive X chromosome alters higher-order genome architecture. *Proc. Natl. Acad. Sci. U.S.A.* **113**, E4504–E4512 (2016).
34. C.-Y. Wang, D. Colognori, H. Sunwoo, D. Wang, J. T. Lee, PRC1 collaborates with SMCHD1 to fold the X-chromosome and spread Xist RNA between chromosome compartments. *Nat. Commun.* **10**, 2950 (2019).
35. C. Perea-Resa, L. Wattendorf, S. Marzouk, M. D. Blower, Cohesin: Behind dynamic genome topology and gene expression reprogramming. *Trends Cell Biol.* **31**, 760–773 (2021).
36. E. Apostolou *et al.*, Genome-wide chromatin interactions of the Nanog locus in pluripotency, differentiation, and reprogramming. *Cell Stem Cell* **12**, 699–712 (2013).
37. H. Zhang *et al.*, Intrachromosomal looping is required for activation of endogenous pluripotency genes during reprogramming. *Cell Stem Cell* **13**, 30–35 (2013).
38. Z. Wei *et al.*, Klf4 organizes long-range chromosomal interactions with the oct4 locus in reprogramming and pluripotency. *Cell Stem Cell* **13**, 36–47 (2013).
39. T. Lavagnolli *et al.*, Initiation and maintenance of pluripotency gene expression in the absence of cohesin. *Genes Dev.* **29**, 23–38 (2015).
40. P. Gupta, T. Lavagnolli, H. Mira-Bontenbal, A. G. Fisher, M. Merkenschlager, Cohesin's role in pluripotency and reprogramming. *Cell Cycle* **15**, 324–330 (2016).
41. A. K. Hadjantonakis, L. L. Cox, P. P. Tam, A. Nagy, An X-linked GFP transgene reveals unexpected paternal X-chromosome activity in trophoblastic giant cells of the mouse placenta. *Genesis* **29**, 133–140 (2001).
42. K. Kurimoto *et al.*, An improved single-cell cDNA amplification method for efficient high-density oligonucleotide microarray analysis. *Nucleic Acids Res.* **34**, e42 (2006).
43. M. Stadtfeld, N. Maherali, M. Borkent, K. Hochedlinger, A reprogrammable mouse strain from gene-targeted embryonic stem cells. *Nat. Methods* **7**, 53–55 (2010).
44. M. Hooper, K. Hardy, A. Handyside, S. Hunter, M. Monk, HPRT-deficient (Lesch-Nyhan) mouse embryos derived from germline colonization by cultured cells. *Nature* **326**, 292–295 (1987).
45. K. Eggan *et al.*, X-Chromosome inactivation in cloned mouse embryos. *Science* **290**, 1578–1581 (2000).
46. K. Takahashi, S. Yamanaka, Induction of pluripotent stem cells from mouse embryonic and adult fibroblast cultures by defined factors. *Cell* **126**, 663–676 (2006).
47. F. Lluis *et al.*, T-cell factor 3 (Tcf3) deletion increases somatic cell reprogramming by inducing epigenome modifications. *Proc. Natl. Acad. Sci. U.S.A.* **108**, 11912–11917 (2011).
48. T. S. Mikkelsen *et al.*, Dissecting direct reprogramming through integrative genomic analysis. *Nature* **454**, 49–55 (2008).
49. T. Sado *et al.*, X inactivation in the mouse embryo deficient for Dnmt1: Distinct effect of hypomethylation on imprinted and random X inactivation. *Dev. Biol.* **225**, 294–303 (2000).
50. J. M. Polo *et al.*, A molecular roadmap of reprogramming somatic cells into iPS cells. *Cell* **151**, 1617–1632 (2012).
51. T. B. Nesterova *et al.*, Pluripotency factor binding and Tsix expression act synergistically to repress Xist in undifferentiated embryonic stem cells. *Epigenet. Chromatin* **4**, 17 (2011).
52. P. Navarro *et al.*, Molecular coupling of Tsix regulation and pluripotency. *Nature* **468**, 457–460 (2010).
53. T. S. Barakat *et al.*, RNF12 activates Xist and is essential for X chromosome inactivation. *PLoS Genet.* **7**, e1002001 (2011).
54. S. Yatskevich, J. Rhodes, K. Nasmyth, Organization of chromosomal DNA by SMC complexes. *Annu. Rev. Genet.* **53**, 445–482 (2019).
55. J.-M. Peters, A. Tedeschi, J. Schmitz, The cohesin complex and its roles in chromosome biology. *Genes Dev.* **22**, 3089–3114 (2008).
56. S. Carvalhal, A. Tavares, M. B. Santos, M. Mirkovic, R. A. Oliveira, A quantitative analysis of cohesin decay in mitotic fidelity. *J. Cell Biol.* **217**, 3343–3353 (2018).
57. M. J. Rust, M. Bates, X. Zhuang, Sub-diffraction-limit imaging by stochastic optical reconstruction microscopy (STORM). *Nat. Methods* **3**, 793–796 (2006).
58. K. Teller *et al.*, A top-down analysis of Xa- and Xi-territories reveals differences of higher order structure at ≥ 20 Mb genomic length scales. *Nucleus* **2**, 465–477 (2011).
59. C. Naughton, D. Sproul, C. Hamilton, N. Gilbert, Analysis of active and inactive X chromosome architecture reveals the independent organization of 30 nm and large-scale chromatin structures. *Mol. Cell* **40**, 397–409 (2010).
60. S. H. Orkin, K. Hochedlinger, Chromatin connections to pluripotency and cellular reprogramming. *Cell* **145**, 835–850 (2011).
61. M. A. Ricci, C. Manzo, M. F. García-Parajo, M. Lakadamyali, M. P. Cosma, Chromatin fibers are formed by heterogeneous groups of nucleosomes in vivo. *Cell* **160**, 1145–1158 (2015).
62. E. G. Schulz *et al.*, The two active X chromosomes in female ESCs block exit from the pluripotent state by modulating the ESC signaling network. *Cell Stem Cell* **14**, 203–216 (2014).
63. J. Song *et al.*, X-chromosome dosage modulates multiple molecular and cellular properties of mouse pluripotent stem cells independently of global DNA methylation levels. *Stem Cell Rep.* **12**, 333–350 (2019).
64. O. Genolet, A. A. Monaco, I. Dunkel, M. Boettcher, E. G. Schulz, Identification of X-chromosomal genes that drive sex differences in embryonic stem cells through a hierarchical CRISPR screening approach. *Genome. Biol.* **22**, 110 (2021).
65. M. Stadtfeld, N. Maherali, D. T. Breault, K. Hochedlinger, Defining molecular cornerstones during fibroblast to iPS cell reprogramming in mouse. *Cell Stem Cell* **2**, 230–240 (2008).
66. R. Li *et al.*, A mesenchymal-to-epithelial transition initiates and is required for the nuclear reprogramming of mouse fibroblasts. *Cell Stem Cell* **7**, 51–63 (2010).
67. P. Samavarchi-Tehrani *et al.*, Functional genomics reveals a BMP-driven mesenchymal-to-epithelial transition in the initiation of somatic cell reprogramming. *Cell Stem Cell* **7**, 64–77 (2010).
68. J. Choi *et al.*, DUSP9 modulates DNA hypomethylation in female mouse pluripotent stem cells. *Cell Stem Cell* **20**, 706–719.e7 (2017).
69. V. Pasque *et al.*, X chromosome dosage influences DNA methylation dynamics during reprogramming to mouse iPSCs. *Stem Cell Rep.* **10**, 1537–1550 (2018).
70. R. Oldenkamp, B. D. Rowland, A walk through the SMC cycle: From catching DNAs to shaping the genome. *Mol. Cell* **82**, 1616–1630 (2022).
71. E.-H. Choi *et al.*, Meiosis-specific cohesin complexes display essential and distinct roles in mitotic embryonic stem cell chromosomes. *Genome Biol.* **23**, 70 (2022).
72. S. S. P. Rao *et al.*, Cohesin loss eliminates all loop domains. *Cell* **171**, 305–320.e24 (2017).
73. J. H. I. Haarhuis *et al.*, The cohesin release factor WAPL restricts chromatin loop extension. *Cell* **169**, 693–707.e14 (2017).
74. J. Nuebler, G. Fudenberg, M. Imakaev, N. Abdennur, L. A. Mirny, Chromatin organization by an interplay of loop extrusion and compartmental segregation. *Proc. Natl. Acad. Sci. U.S.A.* **115**, E6697–E6706 (2018).
75. M. V. Neguembor *et al.*, Transcription-mediated supercoiling regulates genome folding and loop formation. *Mol. Cell* **81**, 3065–3081.e12 (2021).
76. A. Cuadrado *et al.*, Specific contributions of cohesin-SA1 and cohesin-SA2 to TADs and polycomb domains in embryonic stem cells. *Cell Rep.* **27**, 3500–3510.e4 (2019).
77. J. D. P. Rhodes *et al.*, Cohesin disrupts polycomb-dependent chromosome interactions in embryonic stem cells. *Cell Rep.* **30**, 820–835.e10 (2020).
78. B. P. Chadwick, H. F. Willard, Multiple spatially distinct types of facultative heterochromatin on the human inactive X chromosome. *Proc. Natl. Acad. Sci. U.S.A.* **101**, 17450–17455 (2004).
79. A. Cerase *et al.*, Phase separation drives X-chromosome inactivation: A hypothesis. *Nat. Struct. Mol. Biol.* **26**, 331–334 (2019).
80. Y. Markaki *et al.*, Xist nucleates local protein gradients to propagate silencing across the X chromosome. *Cell* **184**, 6174–6192.e32 (2021).
81. A. Cerase, J. M. Calabrese, G. G. Tartaglia, Phase separation drives X-chromosome inactivation. *Nat. Struct. Mol. Biol.* **29**, 183–185 (2022).
82. E. P. Nora *et al.*, Targeted degradation of CTCF decouples local Insulation of chromosome domains from genomic compartmentalization. *Cell* **169**, 930–944.e22 (2017).